CHEMISTRY
A EUROPEAN JOURNAL

DOI: 10.1002/chem.201100583

Self-Assembly of Nanosized 0D Clusters: CdS Quantum Dot–Polyoxotungstate Nanohybrids with Strongly Coupled Electronic Structures and Visible-Light-Active Photofunctions

Hyo Na Kim,[a] Tae Woo Kim,[a] Kyong-Hoon Choi,[b] In Young Kim,[a] Yong-Rok Kim,*[b] and Seong-Ju Hwang*[a]

Abstract: Nanohybrids of CdS–polyoxotungstate with strongly coupled electronic structures and visible-light-active photofunctions can be synthesized by electrostatically derived self-assembly of very small CdS quantum dots, or QDs, (particle size $\approx$2.5 nm) and polyoxotungstate nanoclusters (cluster size $\approx$1 nm). The formation of CdS–polyoxotungstate nanohybrids is confirmed by high-resolution transmission electron microscopy, elemental mapping, and powder X-ray diffraction analysis. Due to the strong electronic coupling between two semiconductors, the CdS–polyoxotungstate nanohybrids show a narrow bandgap energy of around 1.9–2.7 eV, thus reflecting their ability to harvest visible light. Time-resolved photoluminescence experiments indicate that the self-assembly between nanosized CdS and polyoxotungstate is very effective in increasing the lifetime of holes and electrons, thus indicating an efficient electron transfer between two-component semiconductors. The hybridization results not only in a significant improvement in the photostability of CdS QD but also in the creation of visible-light-induced photochromism. Of particular importance is that the present nanohybrids show visible-light-driven photocatalytic activity to produce H_2 and O_2, which is superior to those of the unhybridized CdS and polyoxotungstate. The self-assembly of nanometer-level semiconductor clusters can provide a powerful way of optimizing the photoinduced functionalities of each component (i.e., visible-induced photochromism and photocatalysis) by means of strong electronic coupling.

Keywords: electronic structure · nanostructures · photochromism · polyoxometalates · self-assembly

Introduction

Hybridization between two types of nanostructured materials provides a valuable opportunity to improve the functionality of each component and also to create unexpected novel functions by means of the synergetic combination of two existing properties.[1–5] In one instance, an efficient photodegradation of volatile organic compounds under visible-light illumination can be accomplished by hybridization between the 2D nanosheets of wide-bandgap semiconducting titanate and the 0D nanoclusters of narrow-bandgap semiconducting metal hydroxide.[6–12] To explore new hybrid photocatalysts active for visible-light-induced H_2 production, cadmium sulfide quantum dot, or CdS QD, is supposed to be a useful building block.[13–17] This supposition is based on advantageous electronic characteristics of CdS QD such as narrow-bandgap separation, high quantum yield, and suitable band position for proton reduction.[18–25] Most preparation methods of CdS QD, however, adopt hydrophobic solvent as reaction media,[26–28] and thus the resulting nanoparticles are neither soluble in aqueous media nor have significant surface charge. For this reason, most coupling experiments between metal oxide and cadmium sulfide are carried out by the direct growth of CdS on the surface of metal oxide bulk particles.[15,29] Such a surface sensitization of CdS results in only a limited electronic coupling between the two semiconductors. This synthetic route is not so effective in synthesizing strongly coupled hybrid materials. Alternatively, a solution-based method has been developed for the aqueous suspension of hydrophilic CdS QDs with small diameters of around 2–3 nm.[30] The resulting CdS QD can be positively charged by the anchoring of ammonium groups and thus can readily combine with negatively charged nanoclusters.[31,32] As a candidate for the hybridization with amine-anchored CdS, there are many polyoxometalate, or POM, anions formed by the hydroxylation of metal ions such as W, Mo, and V.[33–35] Most of the POM ions possess intriguing physicochemical characteristics and semiconducting properties; for example, polyoxotungstate cluster anion

[a] H. N. Kim, Dr. T. W. Kim, I. Y. Kim, Prof. S.-J. Hwang
Center for Intelligent Nano-Bio Materials (CINBM)
Department of Chemistry and Nano Sciences
Ewha Womans University, Seoul 120-750 (Korea)
Fax: (+82) 2-3277-4348
E-mail: hwangsju@ewha.ac.kr

[b] Dr. K.-H. Choi, Prof. Y.-R. Kim
Department of Chemistry, Yonsei University
Seoul 120-749 (Korea)
Fax: (+82) 2-364-7050
E-mail: yrkim@yonsei.ac.kr

Supporting information for this article is available on the WWW under http://dx.doi.org/10.1002/chem.201100583.

can be used as an efficient precursor for a nanocrystalline WO_3 material that shows promising photocatalytic activity and photochromic properties.[36–38] Moreover, the uniform small size of polyoxotungstate (<1 nm) renders this species very suitable for coupling with CdS QDs. The electrostatically induced self-assembly between two oppositely-charged 0D nanoclusters with limited crystal dimensions is expected to be highly effective not only in homogeneously hybridizing two different semiconductors on the nanometer-scale but also in enhancing the charge transfer between them and thus tailoring their photoinduced functionalities. At the time of the publication of the present study, however, we are aware of no reports on the self-assembly between semiconducting QDs and polyoxometalate nanoclusters.

Here we report the synthesis of self-assembled CdS-polyoxotungstate nanohybrids in terms of an electrostatic attraction between positively charged CdS 0D QDs and negatively charged polyoxotungstate 0D nanoclusters. Charge transfer and electronic coupling between the two components are investigated with diffuse reflectance UV/Vis spectra and time-resolved photoluminescence, or PL, spectra. The effects of self-assembly on the photocatalytic activity, photochromic properties, and the photostability of component semiconductors are systematically investigated.

Results and Discussion

Powder XRD, HRTEM, and zeta-potential measurements for CdS QDs: As a building block, the amine-anchored CdS QD was synthesized by a solution-based method.[30] This CdS nanoparticle was prepared in the form of a stable colloidal suspension. The crystal structure of precursor CdS QD was examined with powder X-ray diffraction (PXRD). As plotted in Figure 1, the CdS QD shows very broad XRD peaks at $2\theta = 20$–$60°$, which reflects its small particle size. These peaks are indexable with a cubic zinc blend structure and/or a hexagonal wurzite structure. Very broad features of the observed XRD peaks prevented us from conclusively assigning the crystal structure of the obtained CdS QDs. There is another intense peak at the lower angle region of $2\theta \approx 4°$, which can be attributed to the formation of the restacked superstructure of QD nanoparticles.[39] The particle size and shape of the CdS QDs were probed with high-resolution transmission electron microscopy (HRTEM). As illustrated in Figure 1, the obtained CdS QDs showed monodisperse spherical morphology with a particle size of approximately 2.5 nm. Since the surface of the present CdS QD is anchored with amine groups, this material was expected to be positively charged. The positive surface charge of the CdS QDs was confirmed by zeta-potential measurements that showed the positive zeta potential of +50 mV.

PXRD analysis: On the basis of zeta-potential measurements, we tried to combine positively charged CdS QDs with polyoxotungstate anions. The crystal structures of the self-assembled CdS–polyoxotungstate nanohybrid and its calcined derivatives were studied with PXRD, as plotted in Figure 2. The as-prepared nanohybrid displays no well-developed XRD peaks of CdS, polyoxotungstate, and tungsten oxide phases, thus suggesting the nanoscale mixing of both components. After calcination at 330 °C, there is still no distinct peak in the XRD pattern of the nanohybrid. Conversely, the heat treatment at 600–800 °C makes discernible the Bragg reflections of hexagonal CdS and hexagonal WO_3 phases, thereby indicating the improvement of crystallinity of these phases. As the heating temperature was elevated, the XRD peaks became sharper and stronger.

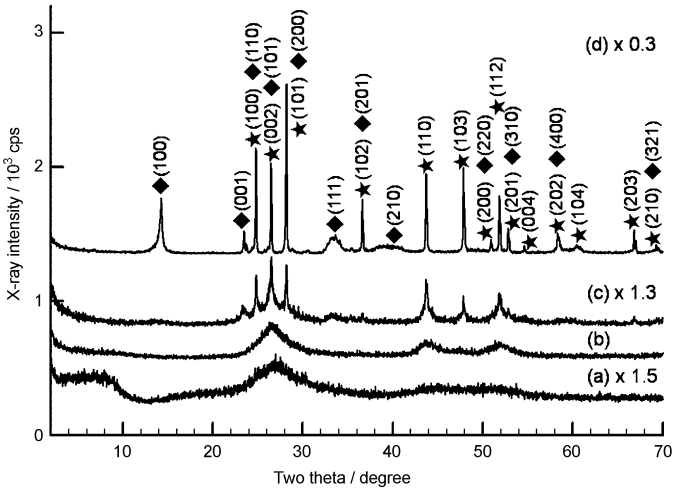

Figure 2. Powder XRD patterns of a) the as-prepared CdS–polyoxotungstate nanohybrid and its derivatives calcined at b) 330, c) 600, and d) 800 °C. In (d), the star and diamond symbols represent the Bragg reflections of hexagonal CdS and hexagonal WO_3 phases, respectively.

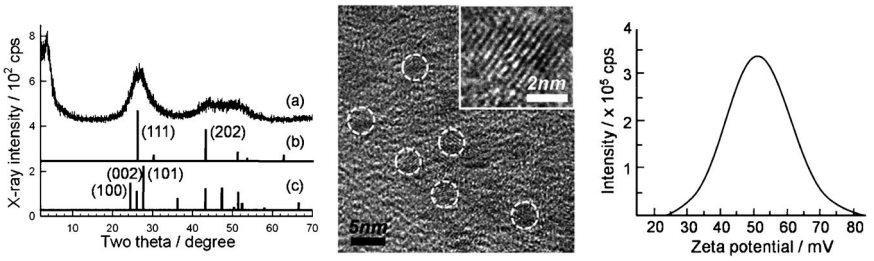

Figure 1. Left: a) Powder XRD pattern of the as-prepared CdS QDs and theoretical Bragg reflection positions of b) cubic CdS and c) hexagonal CdS phases. Center: HRTEM image. Right: zeta-potential curve of the as-prepared CdS QDs.

HRTEM and SAED analyses: The self-assembly between CdS nanoparticles and polyoxotungstate nanoclusters was confirmed by HRTEM analysis. As illustrated in Figure 3, the as-

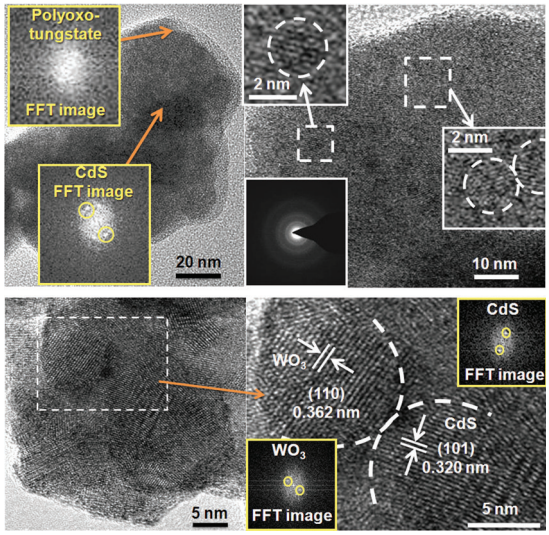

Figure 3. Top: HRTEM and SAED/FFT data of the as-prepared CdS–polyoxotungstate nanohybrid and (bottom) its calcined derivative at 600 °C.

Elemental mapping, TGA, and ICP analyses: To confirm the hybridization between cadmium sulfide and polyoxotungstate, the spatial distributions of Cd, S, W, and O elements in the as-prepared nanohybrid and its calcined derivative were examined with energy-dispersive spectrometry (EDS) and elemental mapping analysis. As illustrated in Figure 4, all of the cadmium, sulfur, tungsten, and oxygen elements are homogeneously distributed in entire parts of the as-prepared CdS–polyoxotungstate nanohybrid, thereby underscoring the homogeneous combination of cadmium sulfide and polyoxotungstate on the nanometer scale. Such a homogeneous distribution of four elements was well maintained after heat treatment at 600 °C. This finding provides strong evidence for the nanoscale mixing between the two species without any spatial separation of cadmium sulfide and tungsten oxide. Our analysis of the inductively coupled plasma (ICP) spectrometry and EDS clearly demonstrated that the as-prepared nanohybrid contains Cd, S, and W with the ratios of Cd/W = 4.53 and S/Cd = 1.14. According to the thermogravimetric analysis (TGA) of the as-prepared CdS–polyoxotungstate nanohybrid,[40] this material showed a considerable mass loss in the temperature range of 25–250 °C, which corresponds to the removal of surface-adsorbed water and hydroxyl groups. Based on the results of ICP and TGA, the chemical formula of the as-prepared nanohybrid was determined to be $4.53[(CdS)(SC_2H_4NH_2)_{0.14}]\cdot W(OH)_{4.64}\cdot 2.12H_2O$.

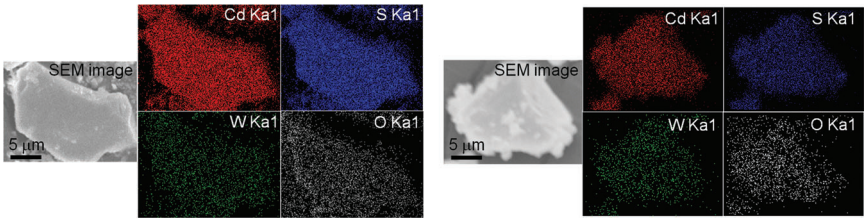

Figure 4. Left: Elemental mapping data of the as-prepared CdS–polyoxotungstate nanohybrid and (right) its calcined derivative at 600 °C.

prepared nanohybrid is composed of the nanoscale mixture of two different domains. The simulation results of the fast Fourier transform (FFT) images clearly demonstrate that the CdS domains show diffraction spots of CdS phase, whereas no clear spots appear for the polyoxotungstate domains. This finding underscores that the as-prepared nanohybrid consists of crystalline CdS domains and poorly crystalline polyoxotungstate domains. After calcination at 600 °C, both domains became highly crystalline. As can be seen clearly in Figure 3, clear lattice fringes are observable in both the domains of cadmium sulfide and tungsten oxide. From the interplanar distances, the observed lattice planes can be indexed as a (101) plane of hexagonal CdS lattice and a (110) plane of hexagonal WO_3 lattice, respectively. The crystallization of both the structures is further confirmed by the observation of diffraction spots in FFT images of both domains and also by diffraction spots of both phases in selected-area electron diffraction (SAED).[40] Before and after the calcinations at $\leq$600 °C, the nanoscale mixing of two materials remained unchanged. The present findings clearly demonstrate that a self-assembly between two oppositely charged nanospecies is quite effective in synthesizing the nanohybrids composed of homogeneously mixed CdS and tungsten oxide nanoparticles. Conversely, the heat treatment at 800 °C induced a distinct phase separation of rod-shaped tungsten oxide crystals and polyhedral cadmium sulfide crystals, as evidenced by field-emission scanning electron microscopy (FE-SEM).[40] Thus, the further characterizations were carried out for the as-prepared nanohybrid and its derivatives calcined at $\leq$600 °C.

Cd K-edge and W L_{III}-edge X-ray absorption near-edge structure (XANES) spectroscopy: The electronic structure and local atomic arrangement of cadmium and tungsten ions in the CdS–polyoxotungstate nanohybrids were investigated with XANES spectroscopy at the Cd K-edge and W L_{III}-edge. The Cd K-edge XANES spectra for the as-prepared CdS–polyoxotungstate nanohybrid, and its calcined derivatives are presented in the left panel of Figure 5 together with the reference spectra of CdO and precursor CdS QD.[41] There are notable differences in the spectral features between the reference CdS and CdO spectra. The spectrum of the as-prepared nanohybrid appears nearly identical in edge position and overall spectral features to that of CdS. Even after the calcination at elevated temperatures, the overall spectral features remained unchanged, which are obviously distinguishable from that of the CdO. There is no

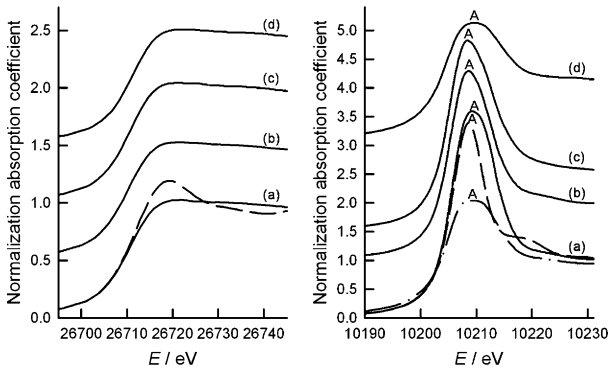

Figure 5. Left: Cd K-edge XANES spectra of a) CdS QD (solid lines)/CdO (dashed lines), and b) the as-prepared CdS–polyoxotungstate nanohybrid and its derivatives calcined at c) 330 and d) 600 °C. Right: W L_{III}-edge XANES spectra of a) the as-prepared CdS–polyoxotungstate nanohybrid (solid lines)/$Na_2WO_4{\cdot}2H_2O$ (dashed lines)/ammonium polyoxotungstate (dot-dashed lines), and the calcined nanohybrids at b) 330 and c) 600 °C, and d) bulk WO_3.

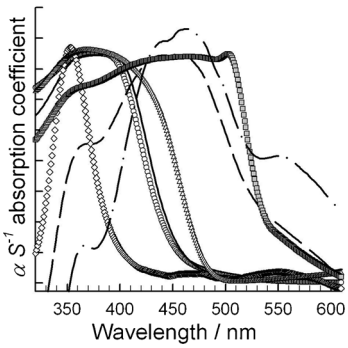

Figure 6. Diffuse reflectance UV/Vis spectra of the as-prepared CdS–polyoxotungstate nanohybrid (solid lines), its calcined derivatives at 330 (dashed lines) and 600 °C (dot-dashed lines), the as-prepared CdS QDs (circles), bulk CdS (squares), ammonium polyoxotungstate (diamonds), and bulk WO_3 (triangles).

marked difference between the spectra of the nanohybrids calcined at 330 and 600 °C, although the XRD analysis for these compounds demonstrates the initiation of the crystallization of cadmium sulfide at temperatures above 600 °C (Figure 2). This finding indicates that CdS in the X-ray amorphous nanohybrids (i.e., the as-prepared and 330 °C-calcined samples) has very similar local atomic arrangement to crystalline CdS, and the heat treatment at elevated temperatures has little influence on the chemical-bonding nature of the CdS component. The right panel of Figure 5 illustrates the W L_{III}-edge XANES spectra of the CdS–polyoxotungstate nanohybrids and some references. There is an intense and broad white-line peak A at around 10210 eV in all the present spectra. This peak is attributed to dipole-allowed transitions from the 2s level to unoccupied 5d states.[36,42] Considering the fact that W 5d orbitals are separated into t_{2g} (or e) and e_g (or t_2) orbitals under an octahedral (or tetrahedral) crystal field, the observed broad peak A for the present tungsten compounds consists of overlapped features that correspond to $2s \rightarrow 5d_{t_{2g}}$ (or $5d_e$) and $2s \rightarrow 5d_{e_g}$ (or $5d_{t_2}$) transitions.[36,43] Since the crystal field of tetrahedral symmetry is weaker than that of the octahedral one,[36,42] the reference $Na_2WO_4{\cdot}2H_2O$ with tetrahedral WO_4 unit shows a narrower full width at half-maximum (FWHM) for the peak A than the reference WO_3 with WO_6 octahedral units. Both the as-prepared and calcined nanohybrids display broader FWHM than $Na_2WO_4{\cdot}2H_2O$, which clearly demonstrates the maintenance of the octahedral symmetry of tungsten ions before and after the calcination.

Diffuse reflectance UV/Vis spectroscopy for CdS–polyoxotungstate nanohybrids: The electronic structure of the CdS–polyoxotungstate nanohybrids was examined with diffuse reflectance UV/Vis spectroscopy. Figure 6 represents diffuse reflectance UV/Vis spectra for the as-prepared CdS–polyoxotungstate nanohybrid and its calcined derivatives relative to several reference spectra. The bandgap energy (E_g) can be estimated by the linear interpolation of α/S absorption coefficients converted from the reflectance data through the Kubelka–Munk function.[44,45] Whereas the bulk CdS has a narrow bandgap energy of 2.3 eV, a larger bandgap energy of approximately 2.9 eV was observed for the CdS QDs due to the quantum confinement effect.[46] As plotted in Figure 6, another precursor of ammonium polyoxotungstate exhibits a bandgap energy of around 3.0 eV. The as-prepared CdS–polyoxotungstate nanohybrid shows a smaller bandgap energy of 2.7 eV, which is compatible with the E_g of CdS QD. The calcinations at 330–600 °C gave rise to a further decrease of E_g to $\leq$1.9 eV. This result clearly demonstrates that the electronic coupling between CdS and polyoxotungstate occurs in the present self-assembled nanohybrid. The decrease of bandgap energy upon heat treatment can be interpreted as a result of an enhanced electronic coupling between the two semiconducting components and/or the crystal growth of CdS QD domains.

Time-resolved PL measurements: The electron transfer between CdS and polyoxotungstate in the as-prepared nanohybrid was investigated by monitoring the time-resolved PL signal of this compound. As plotted in the left panel of Figure 7, the CdS–polyoxotungstate nanohybrid shows much

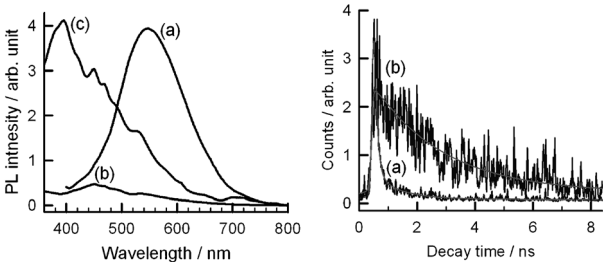

Figure 7. Left: PL spectra for a) CdS QDs, b) the as-prepared CdS–polyoxotungstate nanohybrid, and c) ammonium polyoxotungstate. Right: Time-resolved PL decay curves for a) CdS QDs and b) the as-prepared CdS–polyoxotungstate nanohybrid. The gray lines represent calculated data from the fitting analysis.

slower decay of the PL signals than unhybridized CdS QDs, which strongly suggests the remarkable increase of the lifetime of electrons and holes after the hybridization. According to nonlinear least-squares fitting analysis, the lifetime of electron–hole pair remarkably increases from 84.3 ps for the bare CdS to 2.44 ns for the as-prepared CdS–polyoxotungstate nanohybrid. This finding highlights the high efficiency of electron transfer from the CdS QDs to polyoxotungstate domains, thereby resulting in the effective spatial separation of electrons and holes, and the remarkable depression of their recombination rate. The highly effective electron transfer between the two components is further supported by the dramatic depression of PL intensity after the hybridization. As plotted in the right panel of Figure 7, the present CdS–polyoxotungstate nanohybrid shows a much weaker PL signal than the references CdS QD and polyoxotungstate, thus indicating the effective electron transfer between these two components. The observed weak PL signal of the nanohybrid is also responsible for the poor signal-to-noise ratio in the time-resolved PL decay curves (the left panel of Figure 7). In addition, an intriguing blueshift of the PL emission peak of CdS QD was observed after the hybridization. The energy of the PL peak of the nanohybrid is higher than that of the CdS QD but lower than that of the polyoxotungstate. Although the exact mechanism is not clear at present, we supposed this unique phenomenon to be attributable to the migration of excited electrons from the conduction band (CB) of CdS to that of the polyoxotungstate component and the subsequent electronic transition to unoccupied interband states above the valence band (VB) of polyoxotungstate. To clearly understand this unique observation, further investigations will be required in future.

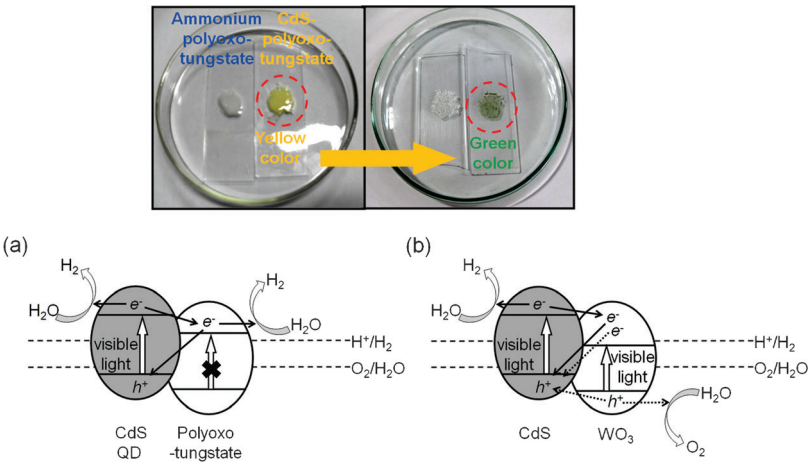

Figure 8. Top: Photochromism images of the as-prepared CdS–polyoxotungstate nanohybrid and ammonium polyoxotungstate (left) before and (right) after visible-light illumination ($\lambda > 420$ nm). Bottom: Schematic models for the electronic structures of a) the as-prepared CdS–polyoxotungstate nanohybrid and b) its calcined derivative.

Photochromic property measurements: To study the effect of CdS hybridization on the electronic structure of the polyoxotungstate component, evolution of photochromic behaviors upon the hybridization was investigated. As illustrated in the left panel of Figure 8, a color change of polyoxotungstate can be induced only by UV irradiation. The observed color change of tungsten compound (i.e., photochromism) occurred through the photoreduction of hexavalent tungsten ions.[47,48] Due to the large bandgap energy of the polyoxotungstate species, no color change occurred under the irradiation of visible light. Conversely, the CdS–polyoxotungstate hybrid displayed a distinct color change from yellow to green under visible illumination ($\lambda > 420$ nm), thus indicating the visible-induced photochromism of the present nanohybrid. The dependence of photochromism behaviors on the wavelength of irradiated beam is summarized in Table 1 for the nanohybrid and ammonium polyoxotungstate (i.e., metatungstate). The observed wavelength dependency of the photochromism is fairly consistent with the change of bandgap energy before and after hybridization. The observed visible-light-induced photochromism of the nanohybrid can be understood by the transfer of excited electrons generated in the CB of the CdS component to that of polyoxotungstate component. Thus, this finding provides another clear piece of evidence for the strong electronic coupling between CdS QDs and polyoxotungstate. Based on the present experimental findings, we suggest schematic models for coupled electronic structures of the CdS–polyoxotungstate nanohybrids. As illustrated in the right panel of Figure 8, due to the relative band positions of CdS and polyoxotungstate, excited electrons in the CdS component can migrate into the CB of the polyoxotungstate component.

Table 1. Energy dependence of the photochromism[a] of the as-prepared CdS-polyoxotungstate nanohybrid and ammonium polyoxotungstate.

λ [nm]	Energy [eV]	CdS–polyoxotungstate nanohybrid	Ammonium polyoxotungstate
295	4.2	○	○
335	3.7	○	○
420	3.0	○	×
430	2.9	○	×
495	2.5	×	×
550	2.3	×	×

[a] ○: Photochromism. ×: No photochromism.

Photostability tests: The photostability of the CdS QDs hybridized with polyoxotungstate was evaluated by monitoring the time-dependent change of their PL signal. The excita-

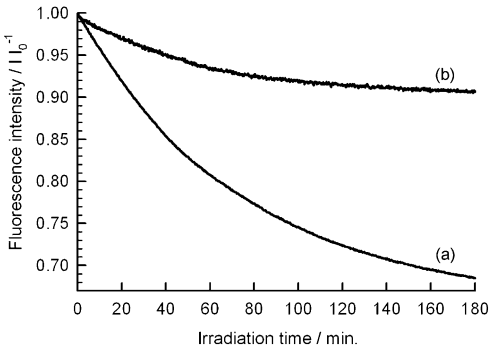

Figure 9. Time-dependent photostability of a) the precursor CdS QDs and b) the as-prepared CdS–polyoxotungstate nanohybrid.

tion wavelength was 385 nm for both the CdS QD and the as-prepared CdS-polyoxotungstate nanohybrid, and the emission wavelengths were 543 and 549 nm, respectively. As plotted in Figure 9, the as-prepared CdS–polyoxotungstate nanohybrid shows a much slower and weaker depression of the PL intensity from the CdS component relative to the precursor CdS QDs. This suggests the stabilization of the CdS QDs by a hole curing by electrons transferred from the polyoxotungstate component. The observed stability improvement can be regarded as another piece of evidence for the strong electronic correlation between CdS and polyoxotungstate components.

Photocatalytic activity measurements: The photocatalytic activity of the as-prepared CdS–polyoxotungstate nanohybrid and its calcined derivatives is tested by monitoring the time-dependent photoproduction of H_2 and O_2 gas in an illuminated catalyst suspension. As plotted in the left panel of Figure 10, all the present nanohybrids can produce H_2 gas under the irradiation of visible light ($\lambda > 420$ nm). The as-prepared nanohybrid exhibits a higher activity for H_2 production than the precursor CdS QDs. This finding highlights the benefit of the hybridization method in improving the photocatalytic activity of the QDs. The observed improvement in photocatalytic activity would be related to the extension of the lifetime of excited electrons by means of the electron transfer between CdS and polyoxotungstate, as evidenced by the PL experiments (Figure 7). Since the CdS component plays a main role in the evolution of H_2 gas, the as-prepared nanohybrid that contains CdS QDs can show a high photocatalytic activity without any heat-treatment step. The photocatalytic activity of the as-prepared nanohybrid could be further improved by the deposition of Pt cocatalyst. After heat treatment at elevated temperatures, the photocatalytic activity of the nanohybrids became depressed. This is attributed to the enlargement of CdS domains. As plotted in the right panel of Figure 10, the CdS–polyoxotungstate nanohybrids also induce the evolution of O_2 gas under visible-light irradiation. The observed photocatalytic activity of the calcined nanohybrids was much higher than those of the as-prepared nanohybrid and ammonium polyoxotungstate. Such a positive effect of the calcination on the O_2 production can be understood by the crystallization of tungsten oxide, since the crystalline tungsten oxide is highly active for the photoproduction of O_2 gas.[49–51] As found in the HRTEM analysis (Figure 3), the as-prepared nanohybrid contains poorly crystalline polyoxotungstate clusters and thus this material shows a low activity for O_2 production. Thus, the observed O_2 production under visible-light illumination can be attributed to the crystallization of WO_3 and/or to an enhanced electronic coupling between narrow-bandgap CdS and tungsten oxide domains, thus resulting in notable decrease in bandgap energy (Figure 6).

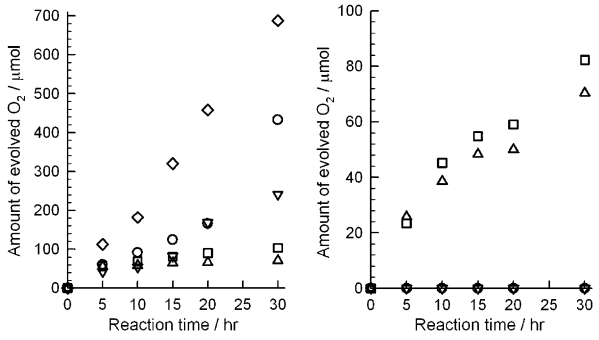

Figure 10. Visible-light ($\lambda > 420$ nm)-induced production of H_2 (left) and O_2 (right) gas by the as-prepared CdS–polyoxotungstate nanohybrid (○), Pt-deposited (3.7 wt %) nanohybrid (◇), the CdS–polyoxotungstate nanohybrids calcined at 330 (△) and 600 °C (□), and reference CdS QD (left, ▽) and ammonium polyoxotungstate (right, ▽).

Conclusion

Self-assembly between positively charged CdS 0D QDs and negatively charged polyoxotungstate 0D nanoclusters produced CdS–polyoxotungstate nanohybrids with efficient internal charge transfer and strong electronic coupling. An electrostatic interaction between two oppositely charged 0D nanoparticles with small crystal sizes was fairly effective in homogeneously hybridizing two kinds of semiconducting materials on the nanometer scale and also in enhancing the charge transfer between the two semiconducting materials. As a consequence of an efficient electronic coupling between these components, the self-assembled CdS–polyoxotungstate nanohybrid can harvest visible light, thereby resulting in visible-light-induced photocatalytic activity and photochromic properties. The present nanohybrids are more active for the photoproduction of H_2 and O_2 gases than the precursors CdS and polyoxotungstate. Also, these materials show a distinct color change under the irradiation of visible light ($\lambda > 420$ nm) and the improved photostability of CdS components. The present experimental findings clearly demonstrate that the electrostatic-interaction-derived self-assembly between two oppositely charged nanoclusters with nanometer-level size can provide a powerful tool to optimize the photoinduced functionalities of wide-bandgap semiconducting nanoparticles as well as to suppress the photocorrosion of narrow-bandgap semiconducting metal chalcogenide. Our

current project is the application of the present methodology to various couples of oppositely charged semiconducting 0D nanoclusters.

Experimental Section

Sample preparation: Amine-modified CdS QD was synthesized by the following procedure:[30] cadmium acetate dehydrate (1.33 g, 5 mmol), 2-mercaptoethylamine hydrochloride (1.42 g, 12.5 mmol), and thioacetamide (0.47 g, 6.25 mmol) were dissolved in deionized water (250 mL). The reaction proceeded at 40 °C for 5 h and then 60 °C for 5 h under vigorous stirring. The resulting solution was filtered and concentrated to around 10–20 mL. After adding isopropyl alcohol, the solution became turbid, and the powdery product was separated by centrifugation. After isolation, the precipitate was redispersed in water and reprecipitated by adding isopropyl alcohol. This process was repeated four times. The precipitate of amine-modified CdS QD was dried in vacuum at 40 °C for 1 d. The self-assembled CdS–polyoxotungstate nanohybrid was synthesized by the following procedure: CdS QD (0.01 mmol) was dispersed in distilled water (20 mL), and ammonium metatungstate (0.03 mmol) was dissolved in the same volume of deionized water. Before the reaction, the pH of the reactant suspension and solution was adjusted to 4 by using concentrated HCl solution. Then, the ammonium metatungstate solution was dropped to the aqueous suspension of CdS QDs at room temperature under vigorous stirring. The reaction was carried out for 2 h, thereby resulting in a yellowish precipitate of the CdS–polyoxotungstate nanohybrid. The obtained product was thoroughly washed with deionized water and dried in vacuum at 40 °C for 1 d. To improve the crystallinity of the CdS–polyoxotungstate nanohybrid, the as-prepared material was heated at 330, 600, and 800 °C under N_2 atmosphere for 3 h.

Sample characterization: The crystal structures of the present nanohybrid materials were studied by powder XRD measurements using a Rigaku diffractometer with Ni-filtered $Cu_{K\alpha}$ radiation ($\lambda = 1.5418$ Å, $T = 298$ K) and a graphite-diffracted beam monochromator. The atomic arrangements of CdS QD and the CdS–polyoxotungstate nanohybrids were probed by performing HRTEM/SAED measurements using a FEI-Tecnai G^2 F20 microscope at an accelerating voltage of 200 kV. A zeta potential of the colloidal suspension of the amine-modified CdS QD was measured using a Nano ZS (Malvern Instruments) zetasizer. The diluted colloidal suspension was kept at 25 °C and started to circulate into the zeta cell. After stabilization for 2 min, the zeta potential of the amine-modified CdS QD was measured. The crystal morphology and spatial elemental distribution of the nanohybrids were probed by FESEM/EDS and elemental mapping analyses using a Jeol JSM-6700F microscope equipped with an energy-dispersive X-ray spectrometer. The chemical compositions of these samples were determined by performing ICP (Perkin–Elmer Optima-4300 DV) and TGA under N_2 atmosphere at the rate of 5 °C min^{-1}. XANES experiments were carried out at the Cd K-edge and W L_{III}-edge by using the EXAFS facility at the Pohang Accelerator Laboratory (PAL; Pohang, Korea) installed at the 7C beam line and operated at 2.5 GeV and 180 mA. The XANES data were collected from the thin layer of powder samples deposited on transparent adhesive tapes in a transmission mode by using gas-ionization detectors. The measurements were carried out at room temperature using an Si(111) single-crystal monochromator. No focusing mirror was used. Higher harmonics were rejected by detuning. All of the present spectra were calibrated by measuring the spectrum of cadmium oxide and sodium tungstate dihydrate. Background correction and normalization were carried out using the WINXAS 2.0 program. Diffuse reflectance UV/Vis spectra of the powdery samples were measured using a Sinco S-4100 spectrometer with an integrating sphere and by adopting $BaSO_4$ as a reference. For time-resolved PL analysis, all the samples were excited by 315 nm pulses generated from a Raman shifter, which was filled with 18 atm of methane gas and pumped by the fourth harmonic (266 nm, FWHM 20 ps, 10 Hz) of a hybrid mode-locked Nd:YAG laser (Continuum, Leopard D10). The PL kinetic profiles were obtained using a picosecond streak camera (Optronis, SCMU-ST-S20) connected to a spectrometer (CVI, DKSP240) and a CCD system (Optronis, SCRU-SE-S). The observed PL decay curves were analyzed by a nonlinear least-squares iterative deconvolution method. For photochromic property measurements, a Newport Xe lamp (450 W) was used. A Perkin–Elmer LS55 fluorescence spectrometer was used to study the photostability of the precursor CdS QD and the as-prepared CdS–polyoxotungstate nanohybrid. Photocatalytic reaction for H_2 production was carried out in a Pyrex reaction cell, and the volume of the cell was 215 mL. The photocatalyst (0.05 g) was suspended in aqueous solution (100 mL). Also, the photocatalytic reaction for O_2 production was carried out in a Pyrex reaction cell, and the volume of the cell was 57.5 mL. The photocatalyst (0.01 g) was suspended in aqueous solution (20 mL). For H_2 generation, a mixed aqueous solution of Na_2S (0.1 M) and Na_2SO_3 (0.02 M) was used, whereas an aqueous $AgNO_3$ solution (0.01 M) was used as the sacrificial reagent for O_2 generation. The suspension was thoroughly degassed with argon for 30 min and irradiated using a Newport Xe lamp (450 W) equipped with an optical cutoff filter ($\lambda > 420$ nm) to eliminate ultraviolet light and a water filter to remove infrared light. During oxygen production, the reactor was in an argon-flow environment. The amount of hydrogen and oxygen evolved was analyzed using a gas chromatograph (Shimadzu GC-2014).

Acknowledgements

This work was supported by Korea Ministry of Environment as "Converging Technology Project" (191-101-001), by National Research Foundation of Korea Grant funded by the Korean Government (KRF-2008-313-C00442), and by National Research Foundation of Korea Grant funded by the Korean Government (2010-0001485). Y.R.K. is thankful for a grant from the Pioneer Research Center Program through the National Research Foundation of Korea funded by the Ministry of Education, Science and Technology (No. 2010-0002190). The experiments at PAL were supported in part by MOST and POSTECH.

[1] X. Qiu, L. Li, C. Tang, G. Li, *J. Am. Chem. Soc.* **2007**, *129*, 11908–11909.
[2] T. Yao, W. Yan, Z. Sun, Z. Pan, B. He, Y. Jiang, H. Wei, M. Nomura, Y. Xie, Y. Xie, T. Hu, S. Wei, *J. Phys. Chem. C* **2009**, *113*, 3581–3585.
[3] S. Guo, Y. Fang, S. Dong, E. Wang, *J. Phys. Chem. C* **2007**, *111*, 17104–17109.
[4] D. Zhao, C. Chen, C. Yu, W. Ma, J. Zhao, *J. Phys. Chem. C* **2009**, *113*, 13160–13165.
[5] J.-K. Lee, W. Lee, T. J. Yoon, G. S. Park, J. H. Choy, *J. Mater. Chem.* **2002**, *12*, 614–618.
[6] T. W. Kim, S. J. Hwang, Y. Park, W. Choi, J. H. Choy, *J. Phys. Chem. C* **2007**, *111*, 1658–1664.
[7] T. W. Kim, M. J. Paek, H. W. Ha, S. H. Hyun, J. H. Choy, S. J. Hwang, *J. Mater. Chem.* **2010**, *20*, 3238–3245.
[8] T. W. Kim, H. W. Ha, M. J. Paek, I. H. Paek, S. H. Hyun, J. H. Choy, S. J. Hwang, *J. Phys. Chem. C* **2008**, *112*, 14853–14862.
[9] T. W. Kim, S. J. Hwang, S. H. Jhung, J. S. Chang, H. Park, W. Choi, J. H. Choy, *Adv. Mater.* **2008**, *20*, 539–542.
[10] T. W. Kim, S. G. Hur, S. J. Hwang, J. H. Choy, *Chem. Commun.* **2006**, 220–222.
[11] T. W. Kim, S. G. Hur, S. J. Hwang, H. Park, W. Choi, J. H. Choy, *Adv. Funct. Mater.* **2007**, *17*, 307–314.
[12] M. J. Paek, T. W. Kim, S. J. Hwang, *J. Phys. Chem. Solids* **2008**, *69*, 1444–1446.
[13] D. Jing, L. Guo, *J. Phys. Chem. C* **2007**, *111*, 13437–13441.
[14] R. M. Navarro, F. Valle, J. L. G. Fierro, *Int. J. Hydrogen Energy* **2008**, *33*, 4265–4273.
[15] Y. L. Lee, C. F. Chi, S. Y. Liau, *Chem. Mater.* **2010**, *22*, 922–927.
[16] X. Zong, G. Wu, H. Yan, J. Ma, J. Shi, F. Wen, L. Wang, C. Li, *J. Phys. Chem. C* **2010**, *114*, 1963–1968.

[17] C. Wang, R. L. Thomson, J. Baltrus, C. Matranga, *J. Phys. Chem. Lett.* **2010**, *1*, 48–53.
[18] R. Baron, C. H. Huang, D. M. Bassani, A. Onopriyenko, M. Zayats, I. Willner, *Angew. Chem.* **2005**, *117*, 4078–4083; *Angew. Chem. Int. Ed.* **2005**, *44*, 4010–4015.
[19] H. Jia, H. Xu, Y. Hu, Y. Tang, L. Zhang, *Electrochem. Commun.* **2007**, *9*, 354–360.
[20] D. Robert, *Catal. Today* **2007**, *122*, 20–26.
[21] D. Kannaiyan, E. Kim, N. Won, K. W. Kim, Y. H. Jang, M. A. Cha, D. Y. Ryu, S. Kim, D. H. Kim, *J. Mater. Chem.* **2010**, *20*, 677–682.
[22] S. Y. Ryu, J. Choi, W. Balcerski, T. K. Lee, M. R. Hoffmann, *Ind. Eng. Chem. Res.* **2007**, *46*, 7476–7488.
[23] S. Y. Ryu, W. Balcerski, T. K. Lee, M. R. Hoffmann, *J. Phys. Chem. C* **2007**, *111*, 18195–18203.
[24] A. L. Silva, S. Y. Ryu, J. Choi, W. Choi, M. R. Hoffmann, *J. Phys. Chem. C* **2008**, *112*, 12069–12073.
[25] X. Wang, G. Liu, Z. G. Chen, F. Li, L. Wang, G. Q. Lu, H. M. Cheng, *Chem. Commun.* **2009**, 3452–3454.
[26] Z. D. Peng, X. Peng, *J. Am. Chem. Soc.* **2001**, *123*, 183–184.
[27] L. Qu, A. Peng, X. Peng, *Nano Lett.* **2001**, *1*, 333–337.
[28] W. W. Yu, X. Peng, *Angew. Chem.* **2002**, *114*, 2474–2477; *Angew. Chem. Int. Ed.* **2002**, *41*, 2368–2371.
[29] E. D. Spoerke, M. T. Lloyd, Y. Lee, T. N. Lambert, B. B. McKenzie, Y. B. Jiang, D. C. Olson, T. L. Sounart, J. W. P. Hsu, J. A. Voigt, *J. Phys. Chem. C* **2009**, *113*, 16329–16336.
[30] S. Chen, K. Kimura, *Chem. Lett.* **1999**, 233–234.
[31] S. Bothra, H. Sur, V. Liang, *Microelectron. Reliab.* **1999**, *39*, 59–68.
[32] M. Anik, *Electrochim. Acta* **2009**, *54*, 3943–3951.
[33] J. H. Son, H. Choi, Y. U. Kwon, *J. Am. Chem. Soc.* **2000**, *122*, 7432–7433.
[34] D. M. Mizrahi, *J. Hazard. Mater.* **2010**, *179*, 495–499.
[35] J. Arichi, M. Mit. Pereira, P. M. Esteves, B. Louis, *Solid State Sci.* **2010**, *12*, 1866–1869.
[36] A. R. Han, S. J. Hwang, H. Jung, J. H. Choy, *Mater. Lett.* **2008**, *62*, 2297–2300.
[37] F. Shiba, M. Yokoyama, Y. Mita, T. Yamakawa, Y. Okawa, *Mater. Lett.* **2007**, *61*, 1778–1780.
[38] X. Z. Li, F. B. Li, C. L. Yang, W. K. Ge, *J. Photochem. Photobiol. A* **2001**, *141*, 209–217.
[39] D. V. Talapin, A. L. Rogach, A. Kornowski, M. Hasse, H. Weller, *Nano Lett.* **2001**, *1*, 207–211.
[40] See the Supporting Information.
[41] T. Arai, T. Ikemoto, A. Hokura, Y. Terada, T. Kunito, S. Tanabe, I. Nakai, *Environ. Sci. Technol.* **2004**, *38*, 6468–6474.
[42] J. H. Choy, Y. I. Kim, J. B. Yoon, S. H. Choy, *J. Mater. Chem.* **2001**, *11*, 1506–1513.
[43] A. Balema, E. Bernierni, E. Burattini, A. Kuzmin, A. Lusis, J. Purans, *Nucl. Instrum. Meth. A* **1991**, *308*, 234–239.
[44] M. K. Arora, N. Sahu, S. N. Upadhyay, A. S. K. Sinha, *Ind. Eng. Chem. Res.* **1999**, *38*, 2659–2665.
[45] M. Nidhin, R. Indumathy, K. J. Sreeram, B. U. Nair, *Bull. Mater. Sci.* **2008**, *31*, 93–96.
[46] A. A. Sirenko, V. I. Belitsky, T. Ruf, M. Cardona, A. I. Ekimov, C. Trallero-Giner, *Phys. Rev. B* **1998**, *58*, 2077.
[47] T. He, J. Yao, *J. Mater. Chem.* **2007**, *17*, 4547–4557.
[48] Y. Shigesato, *Jpn. J. Appl. Phys.* **1991**, *30*, 1457–1462.
[49] W. Erbs, J. Desilvestro, E. Borgarello, M. Grätzel, *J. Phys. Chem.* **1984**, *88*, 4001–4006.
[50] G. R. Bamwenda, K. Sayama, H. Arakawa, *J. Photochem. Photobiol. A* **1999**, *122*, 175–183.
[51] K. Sivula, F. L. Formal, M. Grätzel, *Chem. Mater.* **2009**, *21*, 2862–2867.

Received: February 22, 2011
Published online: July 20, 2011

